Tunable near-infrared perfect absorber based on the hybridization of phase-change material and nanocross-shaped resonators

Ce Li, Wei Zhu, Zhe Liu, Shi Yan, Ruhao Pan, Shuo Du, Junjie Li, and Changzhi Gu

Citation: Appl. Phys. Lett. **113**, 231103 (2018); doi: 10.1063/1.5063481
View online: https://doi.org/10.1063/1.5063481
View Table of Contents: http://aip.scitation.org/toc/apl/113/23
Published by the American Institute of Physics

Tunable near-infrared perfect absorber based on the hybridization of phase-change material and nanocross-shaped resonators

Ce Li,[1,2] Wei Zhu,[1,3] Zhe Liu,[1,4] Shi Yan,[1] Ruhao Pan,[1,2] Shuo Du,[1,2] Junjie Li,[1,2] and Changzhi Gu[1,2,5,a)]

[1]*Beijing National Laboratory for Condensed Matter Physics, Institute of Physics, Chinese Academy of Sciences, Beijing 100190, China*
[2]*School of Physical Sciences, CAS Key Laboratory of Vacuum Physics, University of Chinese Academy of Sciences, Beijing 100049, China*
[3]*Key Laboratory of Space Applied Physics and Chemistry, Ministry of Education and Department of Applied Physics, School of Science, Northwestern Polytechnical University, Xi'an 710129, China*
[4]*Niels Bohr Institute, University of Copenhagen, Blegdamsvej 17, DK-2100 Copenhagen, Denmark*
[5]*Collaborative Innovation Center of Quantum Matter, Beijing, China*

(Received 27 September 2018; accepted 15 November 2018; published online 4 December 2018)

$Ge_2Sb_2Te_5$ (GST) is a kind of non-volatile chalcogenide phase-change material, which has a significant difference in permittivity between its amorphous and crystalline states in the infrared range. On account of this remarkable property, the combination of GST and metamaterials has great potential in tunable meta-devices. In this paper, a perfect absorber based on a nanocross-resonator array stacked above a GST spacer layer and an Au mirror (i.e., a metal-dielectric-metal configuration) is designed and experimentally demonstrated. A thin indium tin oxide (ITO) protective layer is inserted between the GST spacer and the Au resonator to avoid heat-induced oxidation of the GST layer during phase transition. We found that the ITO layer not only can protect the GST layer from deterioration, but also allows a significant blue shift in the absorption peak from 1.808 μm to 1.559 μm by optimizing the thickness of the two dielectric layers without scaling down the size of the metal structure, which provides a more feasible idea in pushing the absorption peak to higher frequency. The *LC* circuit model is presented to explain this blue-shift phenomenon, which is mainly attributed to the engineering of the dielectric environment of the parallel plate capacitance. In addition, such good performance in dynamitic modulation makes this perfect absorber a robust candidate for optical switching and modulating in various situations. *Published by AIP Publishing.*
https://doi.org/10.1063/1.5063481

Electromagnetic metamaterials,[1,2] a kind of artificial structure with a specified geometry, can yield novel responses to electric and magnetic components of light.[3] In recent years, tunable metamaterials have received extensive attention from researchers due to their unique property of dynamic modulation which has a great significance in expanding their applications.[4] Up to now, one of the most effective ways to achieve dynamic modulation can be attributed to the hybridization of metamaterials with functional materials including graphene,[5–8] semiconductors,[9–12] liquid crystals,[13–16] and phase-change materials.[17–21] The optical or electrical properties of these materials can be modified by a variety of means such as temperature, machining, light, or electric field. By these methods, the dielectric environment[13–21] or the configuration[22–24] of metamaterials can be tuned in a controllable way and thereby dynamic modulation is ultimately realized. However, a majority of these functional materials are difficult to construct scalable metamaterials with tunable frequencies much higher than the THz region due to their low carrier densities.[4] Although liquid crystals have been demonstrated to be able to tune the optical property of metamaterials dynamically in the near infrared range by changing the orientation of constituent molecules,[13,16] they are temperature-sensitive and volatile, which means that the tuned optical properties will return to their original state once the external stimuli are removed. Therefore, a non-volatile metamaterial with preservable optical properties is highly needed for specific applications.

The utilization of PCM for the optical modulation of metamaterials has received widespread attention in recent years. Among them, $Ge_2Sb_2Te_5$ (GST) is extremely scalable, non-volatile, and easily integrated in commercial devices[25,26] with great potential in applications focused on data storage,[27] solid-state and flexible displays,[25] and algorithm processing.[28] GST is a kind of phase-change chalcogenide alloy with both a stable amorphous state and crystalline state at room temperature. It has extraordinary properties such as a fast switching speed and high switching endurance.[29] The phase transition of GST is a thermally determined process, which can be completed by not only direct heating,[30,31] but also laser irradiation[19,32,33] or external electric field[34,35] at the nanosecond or even femtosecond time scale. As a result, the optical and electrical properties of GST will make a tremendous difference between their two states. In optics aspects, this mainly concentrates on the obvious difference in the refractive index and extinction coefficient, which provides the basis for the preparation of dynamic tunable devices by combining GST with metamaterials.[21,31,36,37]

In this paper, a GST based metamaterial perfect absorber (MPA) with a sandwiched "Au film—GST active dielectric layer—nanocross-resonator Au array" configuration was

a)Author to whom correspondence should be addressed: czgu@iphy.ac.cn

proposed and experimentally verified. The total thickness of the entire structure is 180 nm, well below the subwavelength scale. Here, the nanocross-shaped configuration brings about more degrees of freedom (width w) in comparison to the previous patches[36] or nanodisk[31] structures, which allows more control of the reflected light, such as the reflection phase,[38] though here, more attention is still focused on the reflection intensity of the structures. At normal incidence, strong absorption can be generated at the resonant wavelength of 1.808 μm when GST is in the amorphous state. In order to realize a stable phase transition, a 6 nm thick ITO protective layer is inserted between the original GST layer and the Au structure layer. Near perfect absorption at around 1.550 μm, a commonly used wavelength for optical communication and optical signal processing, is achieved by optimizing the thickness of the GST and ITO layer without shrinking the size of the metal structure, though it has been proved that perfect absorption can be realized at any frequency by following simple scaling laws.[39] By converting GST from the amorphous to crystalline state, obvious absorption still exists but a significant red shift occurs simultaneously. Based on this apparent difference in the absorption spectra between these two states of the MPA, such a device is a suitable candidate for an optical modulator, where an extinction ratio of −8.1 dB at the resonance of a-GST has been experimentally achieved, satisfying the need for a typical design target for practicable modulators.[19,40]

The schematic of the GST-based MPA is shown in Fig. 1(a). The total structure employed in this work has a typical metal-dielectric-metal (MIM) configuration which consists of a nanocross-resonator Au array stacked above a 40-nm GST active dielectric layer and a 100-nm-thick bottom Au mirror layer. The nanocross-shaped structure has a period of $p = 320$ nm with length $l = 190$ nm, width $w = 60$ nm, and thickness $t = 40$ nm. Figures 1(b) and 1(c) present the top view and side view of the unit cell of the structures.

The designed structure is implemented by nanofabrication. To begin with, a 100-nm-thick Au film and a 40-nm-thick GST film were deposited successively on an Si substrate

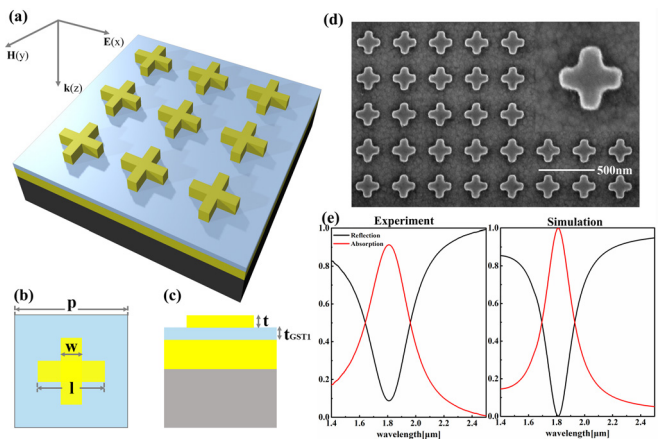

FIG. 1. (a) Schematic of nanocross-shaped MPA and the incident light polarization configuration. (b) and (c) Top view and side view of the MPA unit cell, its optimized dimensions are $p = 320$ nm, $l = 190$ nm, $w = 60$ nm, $t = 40$ nm, and $t_{GST1} = 40$ nm. (d) SEM image of the periodically patterned arrays. (e) Experimental and simulated performance for sample 1, the black line and the red line are the reflection and absorption spectra, respectively.

by direct current (DC) and radio frequency (RF) magnetron sputtering (MS) methods. The deposition of GST is performed from a synthesized single target with the growth pressure at 1 mTorr by a throttle valve with an argon (Ar) gas flow rate of 10 sccm and growth power at 100 W. Both the Au film and the GST film were grown at room temperature, and thus the resulting GST exhibited an amorphous state. The pattern of nanocross-shaped structures was obtained by the electron-beam lithography (EBL) technique. Here, a PMMA (polymethylmethacrylate) bilayer (495 000 A2 at 4000 rpm and 950 000 A5 at 6000 rpm) was spin-coated and baked for 30 min at 100 °C for each layer to prevent the phase change of GST caused by the regular high temperature of the pre-baking process. After development, the 3 nm Cr and 40 nm Au films were deposited using electron-beam evaporation (EBE), followed by a lift-off procedure in 60 °C acetone. The total array size is 80 μm × 80 μm. Figure 1(d) shows the scanning electron microscopy (SEM) image of the fabricated samples for amorphous GST (this sample is named as sample 1).

A 6 nm ITO protective layer was deposited by ion beam sputtering deposition (IBSD) on another sample before the pattern fabrication process. Both the IBSD and the MS are integrated in an ultrahigh-vacuum deposition system, which means that all of the films can be deposited in the same chamber and the oxidation of GST is effectively avoided. The deposition rates of both GST and ITO layers were calibrated by Atomic Force Microscopy (AFM). The thickness of the GST layer is shrunk to 34 nm to obtain the optimal absorptive behavior, and the size of nanocross-shaped Au structures remains unchanged (the sample with the ITO protective layer and thinner GST layer is named as sample 2).

To be converted to the crystalline state, GST needs to be heated above its crystallization temperature (Tcr ∼ 160 °C). In this work, an annealing process at 200 °C was performed in a rapid thermal annealing (RTA) system under a nitrogen atmosphere for 5 min to ensure that the GST is fully crystallized. Only sample 2 participated in the phase transition. The reflection spectra were recorded by a Fourier transform infrared spectrometer (FTIR) with a KBr beam splitter at room-temperature.

Numerical simulations were carried out by using the commercial full-wave simulation software CST Microwave Studio based on the finite integration method to calculate the optical responses of the GST-based MPA. The permittivity of bulk Au is described by the Drude model with plasma frequency $\omega_p = 1.37 \times 10^{16}$ rad/s and collision frequency $\gamma = 4.08 \times 10^{13}$ s^{-1}. The collision frequency used in the simulation is 3 times of that in the real bulk material,[41] taking the surface scattering and grain boundary effects in the thin gold film into account.[42] The optical constants of ITO are chosen from the CST software database. The dispersion relationships of GST in the amorphous state (a-GST) and the crystalline state (c-GST) are extracted from Ref. 43. Periodic boundary conditions were applied to both the x-direction and y-direction, and an open boundary was imposed in the z-direction.

The experimental and simulated results for sample 1 and sample 2 are shown in Figs. 1(e) and 2, respectively. The 100 nm thick bottom Au film is much thicker than the penetration depth of light in the infrared range, therefore, the

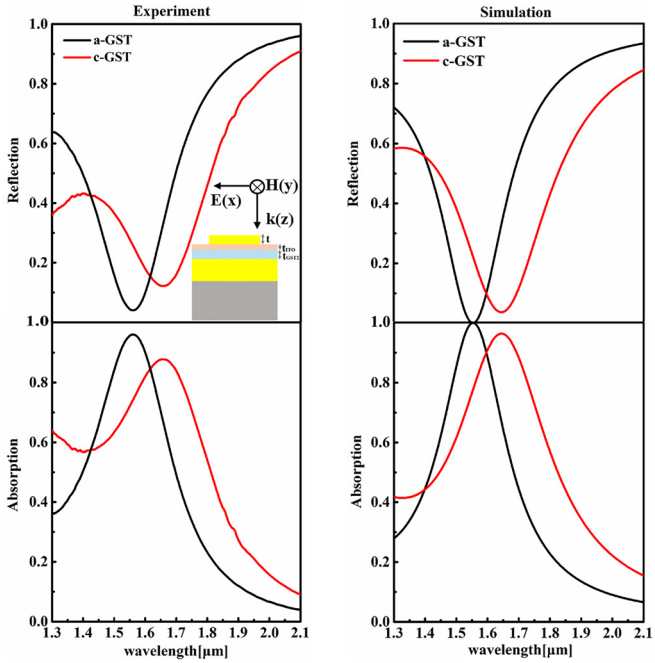

FIG. 2. The experimental and simulated spectra for sample 2 with a 6 nm ITO protective layer inserted between the GST layer and the cross-shaped structure layer. The black line and red line are for the a-GST and c-GST sample. The inset shows the side view of the unit cell, and the thicknesses of the GST and ITO layer are $t_{GST2} = 34$ nm and $t_{ITO} = 6$ nm, respectively. The size of top Au structures remains unchanged.

transmission of the device can be ignored, then the frequency dependent absorption can be calculated as $A(\omega) = 1 - R(\omega)$, where $A(\omega)$ and $R(\omega)$ represent absorption and reflection of the MPA, respectively. In this way, by optimizing the dielectric layer thickness and the structure size, near perfect absorption can be realized at a specific frequency (wavelength) when the reflection is minimized through impedance matching to free space.[44]

For sample 1, the absorption peak appears at the resonant wavelength of 1.808 μm, with an absorption of 91.2% for the experimental result. After the introduction of the ITO protective layer for sample 2, the absorption peak shifts to 1.559 μm and the absorption reaches 96.2%.

Phase transition brings about dramatic changes in the dispersion of GST with a larger refractive index and higher losses in the crystalline state, which causes a strong spectral shift and a certain degree of broadening in the reflection and absorption spectrum, as shown in Fig. 2. After phase transition by rapid annealing for sample 2, perfect absorption undergoes an obvious red shift to 1.654 μm ($\Delta\lambda = 95$nm), with an absorption of 88.1%. For the simulated results, resonance shifts from 1.553 μm with near unity absorption to 1.645 μm ($\Delta\lambda = 92$nm) with an absorption of 96.6%. A good agreement between the experimental and simulated results has been achieved for both a-GST and c-GST. A slight difference in shifts of resonance and decrease in absorption may be attributed to the slight discrepancy in dispersion of GST and the imperfection in fabrication.

In order to investigate the underlying absorption mechanism of the GST-based MPA, the magnetic field and electric-field vector distribution in the TM configuration at the resonant wavelength was calculated as shown in Fig. 3(a). The

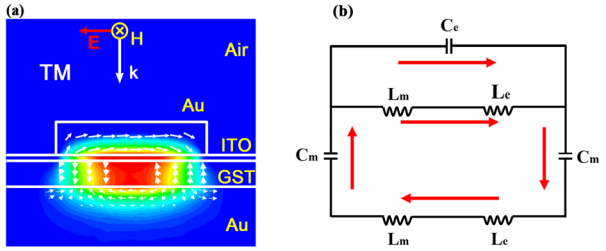

FIG. 3. (a) The magnetic field distribution at the resonance for a-GST sample; the white arrows represent the electric-field distribution. (b) Schematic of the equivalent *LC* circuit for one period of the MPA.

fundamental magnetic mode is generated at the resonance. It is evident that the two metal layers sustain anti-parallel current, producing a magnetic field confined mainly in the dielectric spacer underneath the top Au antenna. The considered structure acts similar to the metal antenna pairs regarding the magnetic field distribution,[45] and hence, it can be regarded that opposite charges accumulated at the ends of the two metal antennas and the electric field are expected to be confined within the space between the antennas and near the end points.

Such field configurations for the fundamental magnetic resonant mode can be accounted for by the equivalent *LC* circuit model. Based on this model, a reasonable interpretation for the blue shift of the absorption peak after the introduction of the ITO protective layer was provided, where the ITO layer can be regarded as a capacitor connected in series with the original capacitor. This gives rise to the decrease in the total capacitance and results in the blue shift of the absorption peak. A more detailed discussion is as follows.

The equivalent *LC* circuit of the MPA is shown in Fig. 3(b). For simplification, two hypotheses are put forward before the interpretation. First, the nanocross-shaped structure can be equivalent to a metal antenna with an effective length l_{eff},[46] and second, the magnetic field between the two metal layers is assumed to be uniform.[47] Hence, L_m, the inductance of the two plates, can be calculated by the magnetic field energy, $L_m = \frac{\mu_0 d l_{eff}}{2w}$, where l_{eff} is the effective length of the equivalent antenna, d is the thickness of the dielectric layer, and μ_0 is the permeability of vacuum. L_e is the inductance attributed to the kinetic energy of the drifting electrons which cannot be ignored in nanoscale metal patches.[48] L_e is expressed as $L_e = \frac{l_{eff}}{\gamma t w \omega_p^2 \varepsilon_0}$, where γt is the effective thickness of the Au structure and $\omega_p = 1.37 \times 10^{16}$ rad/s is the plasma frequency of gold. C_m is the capacitance between two parallel plates sandwiched by the dielectric spacer, which can be given by $C_m = \frac{c_1 \varepsilon w l_{eff}}{d}$, where $0.2 \le c_1 \le 0.3$ is a numerical factor that accounts for the effective area of the capacitor on the metallic antennas.[40] In addition, the capacitance C_e can be approximated by that of two adjacent parallel gold nanorods with radius t_3 and length w at a distance $b = p - l$ apart, $C_e = \frac{\pi \varepsilon w}{\ln(b/t)}$.

According to the *LC* circuit shown in Fig. 3(b), the total impedance Z can be expressed as

$$Z^{-1} = j\omega C_e + \frac{1}{j\omega(L_m + L_e)} + \frac{1}{\frac{2}{j\omega C_m} + j\omega(L_m + L_e)}, \quad (1)$$

where ω is the angular frequency. The magnetic resonance occurs when $Z = 0$, and in this way, the resonance condition can be derived as

$$\omega = \sqrt{\frac{2}{C_{\mathrm{m}}(L_{\mathrm{m}} + L_{\mathrm{e}})}}. \tag{2}$$

As shown in Eq. (2), the resonant frequency ω is related to C_{m}. The introduction of the ITO layer makes an inevitable change in the capacitor C_{m}, where the ITO layer and the GST layer can be regarded as a series connection of two capacitors with the thickness and permittivity t_{ITO}, $\varepsilon_{\mathrm{ITO}}(\omega)$ and t_{GST2}, $\varepsilon_{\mathrm{GST2}}(\omega)$, respectively. In this way, the total capacitance of C_{m2} for sample 2 can be expressed as $C_{m2} = \frac{1}{\frac{1}{C_{\mathrm{mITO}}} + \frac{1}{C_{\mathrm{mGST}}}} = \frac{wl_{\mathrm{eff}}}{\frac{t_{\mathrm{ITO}}}{\varepsilon_{\mathrm{ITO}}(\omega)} + \frac{t_{\mathrm{GST2}}}{\varepsilon_{\mathrm{GST}}(\omega)}}$. The dielectric thickness of sample 2 ($t_{\mathrm{ITO}} + t_{\mathrm{GST2}}$) is equal to that of sample 1 ($t_{\mathrm{GST1}} = t_{\mathrm{ITO}} + t_{\mathrm{GST2}} = 40\,\mathrm{nm}$), and thus, the inductance $L_{\mathrm{m}} + L_{\mathrm{e}}$ can be regarded as the same for both the samples. Therefore, the ratio of the resonant frequency for sample 2 (ω_2) and sample 1 (ω_1) is

$$\frac{\omega_2}{\omega_1} \approx \sqrt{\frac{C_{\mathrm{m1}}}{C_{\mathrm{m2}}}} = \sqrt{\frac{\varepsilon_{\mathrm{GST}}(\omega_1)}{t_{\mathrm{GST1}}} \cdot \left(\frac{t_{\mathrm{ITO}}}{\varepsilon_{\mathrm{ITO}}(\omega_2)} + \frac{t_{\mathrm{GST2}}}{\varepsilon_{\mathrm{GST2}}(\omega_2)}\right)}$$
$$\approx 1.18. \tag{3}$$

The predicated ratio of the resonant wavelength based on the equivalent *LC* circuit is compared with that obtained from the simulated result, where

$$\frac{\omega_2}{\omega_1} = \frac{\lambda_1}{\lambda_2} \approx 1.16. \tag{4}$$

It is apparent that the predicated result is in good agreement with the simulated result according to Eqs. (3) and (4), which corroborates that the *LC* circuit can be unutilized to interpret this blue-shift phenomenon.

On the other hand, as it was verified in Fig. 2, the phase transition of GST gave rise to a tremendous discrepancy in spectra, which indicates that such GST based MPA can be utilized as an optical modulator. Two appropriate figures of merit, modulation depth (*MD*), and extinction ratio (*ER*) are introduced here to characterize the performance of an optical modulator quantitatively.[37] *MD* is defined as the difference between the maximum reflection $R_{\mathrm{on}}(\lambda)$ (corresponding to c-GST) and the minimum reflection $R_{\mathrm{off}}(\lambda)$ (corresponding to a-GST), normalized by the maximum reflection $R_{\mathrm{on}}(\lambda)$. *ER* is defined as the logarithm of the ratio of the maximum to the minimum reflection. The formulas of the wavelength-dependent on *MD* and *ER* are as follows:[5]

$$MD = \frac{R_{\mathrm{on}}(\lambda) - R_{\mathrm{off}}(\lambda)}{R_{\mathrm{on}}(\lambda)} = \frac{R_{\mathrm{c-GST}}(\lambda) - R_{a-\mathrm{GST}}(\lambda)}{R_{\mathrm{c-GST}}(\lambda)}, \tag{5}$$

$$ER = -10\lg\frac{R_{\mathrm{on}}(\lambda)}{R_{\mathrm{off}}(\lambda)} = -10\lg\frac{R_{\mathrm{c-GST}}(\lambda)}{R_{\mathrm{a-GST}}(\lambda)}. \tag{6}$$

It is evident that the higher is the ratio of $R_{\mathrm{c\text{-}GST}}(\lambda)$ to $R_{\mathrm{a\text{-}GST}}(\lambda)$, the more distinguishing is the reflection difference and the better performance the optical modulator shows. The *MD* and *ER* for the experimental and simulated results are plotted in Fig. 4. The curves show clearly that at the resonance of a-GST, both the *MD* and *ER* reach a maximum, representing the best modulation performance. The

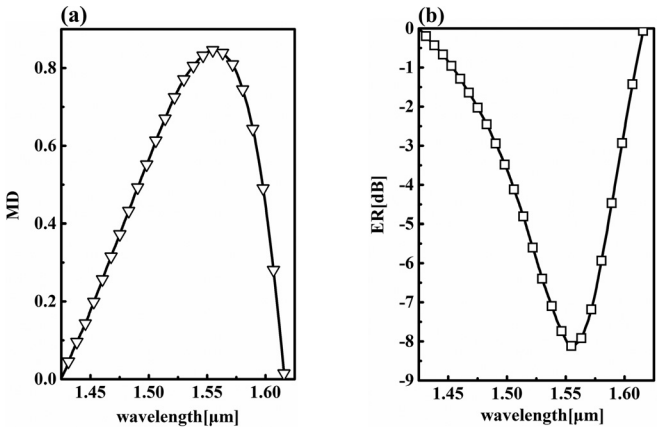

FIG. 4. (a) Experimental *MD* and (b) *ER* as a function of wavelength; the optimal values of the *MD* and *ER* are reached at the resonance of a-GST.

MD and *ER* reached 85% and −8.1 dB in the experiment, respectively, which greatly satisfied the typical design target for practical modulators.

In conclusion, a tunable GST-based MPA in the near infrared region was demonstrated. We proved that the introduction of the ITO protective layer can not only prevent GST from oxidation during the phase transition, but also give rise to the blue shift of the resonant wavelength by merely optimizing the thickness of the ITO layer and GST layer without scaling down the metal structure size. The *LC* circuit model is introduced to explain this phenomenon, which has a good agreement with the simulated and experimental results. Dielectric environment engineering, which is equivalent to tuning the permittivity of the capacitance of the *LC* circuit, will inevitably result in the change of resonance. We also proved that such a kind of device was suitable for an optical modulator by taking advantage of the significant difference in the absorption spectrum at the a-GST resonance, where a modulation depth of 85% and an extinction ratio of −8.1 dB were achieved. As a non-volatile, repeatable phase change material, GST has great potential in dynamic optical devices. It is of great significance to further study the repetitive and bidirectional phase transition of GST through electrical or optical methods to achieve the purpose of repeatable dynamic metamaterials.

This work was supported by the National Key Research and Development Program of China (Grant Nos. 2016YFA0200400 and 2016YFA0200800), the National Natural Science Foundation of China (Grant Nos. 91323304, 11674387, 11504414, 11574369, 11574385, 11574369, and 61390503), the Strategic Priority Research Program of the Chinese Academy of Sciences (Grant No. XDB07020200), and the Key Research Program of Frontier Sciences, CAS (Grant No. QYZDJ-SSW-SLH042).

[1]D. R. Smith, B. J. Pendry, and M. C. Wiltshire, Science **305**, 788 (2004).
[2]V. M. Shalaev, Nat. Photonics **1**, 41 (2007).
[3]A. Pandey and S. B. Rana, Res. Cell: Int. J. Eng. Sci. **17**, 359 (2016), available at http://www.ijoes.vidyapublications.com/paper/Vol17/53-Vol17.pdf.
[4]K. Fan and W. J. Padilla, Mater. Today **18**, 39 (2015).
[5]N. Dabidian, I. Kholmanov, A. B. Khanikaev, K. Tatar, S. Trendafilov, S. H. Mousavi, C. Magnuson, R. S. Ruoff, and G. Shvets, ACS Photonics **2**, 216 (2015).

[6]L. Ju, B. Geng, J. Horng, C. Girit, M. Martin, Z. Hao, H. A. Bechtel, X. Liang, A. Zettl, R. Shen *et al.*, Nat. Nanotechnol. **6**, 630 (2011).
[7]T. Low and A. Phaedon, ACS Nano **8**, 1086 (2014).
[8]Z. Fang, Y. Wang, A. E. Schather, Z. Liu, P. M. Ajayan, F. J. G. de Abajo, P. Nordlander, X. Zhu, and N. J. Halas, Nano Lett. **14**, 299 (2014).
[9]H. T. Chen, P. Sabarni, T. Talmage, M. B. Christropher, M. O. Zide, J. F. O'Hara, D. R. Smith, A. C. Gossard, R. D. Averitt, W. J. Padilla *et al.*, Appl. Phys. Lett. **93**, 091117 (2008).
[10]H. T. Chen, J. P. Willie, M. O. Zide, C. G. Arthur, J. T. Antoinette, and D. A. Richard, Nature **444**, 597 (2006).
[11]Q. F. Xu, B. Schmidt, S. Pradhan, and M. Lipson, Nature **435**, 325 (2005).
[12]J. Gu, R. Singh, X. Liu, X. Zhang, Y. Ma, S. Zhang, S. A. Maier, Z. Tian, A. K. Azad, H. T. Chen *et al.*, Nat. Commun. **3**, 1151 (2012).
[13]B. Kang, J. H. Woo, E. Choi, H. H. Lee, E. S. Kim, J. Kim, T. J. Hwang, Y. S. Park, D. H. Kim, and J. W. Wu, Opt. Express **18**, 16492 (2006).
[14]D. Shrekenhamer, W. C. Chen, and W. J. Padilla, Phys. Rev. Lett. **110**, 177403 (2013).
[15]Q. Zhao, L. Kang, B. Du, B. Li, J. Zhou, H. Tang, X. Liang, and B. Zhang, Appl. Phys. Lett. **90**, 011112 (2007).
[16]X. Wang, D. H. Kwon, D. H. Werner, I. C. Khoo, A. V. Kildishev, and V. M. Shalaev, Appl. Phys. Lett. **91**, 143122 (2007).
[17]X. Duan, S. Chen, H. Cheng, Z. Li, and J. Tian, Opt. Lett. **38**, 483 (2013).
[18]M. A. Kats, R. Blanchard, P. Genevet, Z. Yang, M. M. Qazilbash, D. N. Basov, S. Ramanathan, and F. Capasso, Opt. Lett. **38**, 368 (2013).
[19]B. Gholipour, J. Zhang, K. F. MacDonald, D. W. Hewak, and N. I. Zheludev, Adv. Mater. **25**, 3050 (2013).
[20]T. Cao, C. Wei, R. E. Simpson, L. Zhang, and M. J. Cryan, Opt. Mater. Express **3**, 1101 (2013).
[21]W. Zhu, R. Yang, Y. Fan, Q. Fu, H. Wu, P. Zhang, N. Shen, and F. Zhang, Nanoscale **10**, 12054 (2018).
[22]T. Hand and S. Member, IEEE Antennas Wireless Propag. Lett. **6**, 401 (2007).
[23]H. Tao, A. C. Strikwerda, K. Fan, W. J. Padilla, X. Zhang, and R. D. Averitt, Phys. Rev. Lett. **103**, 147401 (2009).
[24]C. M. Watts, X. Liu, and W. J. Padilla, Adv. Mater. **24**, 98 (2012).
[25]P. Hosseini, C. D. Wright, and H. Bhaskaran, Nature **511**, 206 (2014).
[26]S. H. Lee, Y. Jung, and R. Agarwal, Nat. Nanotechnol. **2**, 626 (2007).
[27]M. Wuttig and N. Yamada, Nat. Mater. **6**, 824 (2007).
[28]C. D. Wright, Y. Liu, K. I. Kohary, M. M. Aziz, and R. J. Hicken, Adv. Mater. **23**, 3408 (2011).
[29]M. A. Caldwell, R. G. D. Jeyasingh, H. S. P. Wong, and D. J. Milliron, Nanoscale **4**, 4382 (2012).
[30]B. Liu, T. Zhang, J. Xia, Z. Song, S. Feng, and B. Chen, Semicond. Sci. Technol. **19**, L61 (2004).
[31]Y. Qu, Q. Li, K. Du, L. Cai, J. Lu, and M. Qiu, Laser Photonics Rev. **11**, 1700091 (2017).
[32]Q. Wang, E. T. F. Rogers, B. Gholipour, C. M. Wang, G. Yuan, J. Teng, and N. I. Zheludev, Nat. Photonics **10**, 60 (2016).
[33]A. K. U. Michel, P. Zalden, D. N. Chigrin, M. Wuttig, A. M. Lindenberg, and T. Taubner, ACS Photonics **1**, 833 (2014).
[34]H. Satoh, K. Sugawara, and K. Tanaka, J. Appl. Phys. **99**, 024306 (2006).
[35]Y. Hu, H. Zou, J. Zhang, J. Xue, Y. Sui, W. Wu, L. Yuan, X. Zhu, S. Song, and Z. Song, Appl. Phys. Lett. **107**, 263105 (2015).
[36]A. Tittl, A. U. Michel, M. Schaferling, X. Yin, B. Gholipour, L. Cui, M. Wuttig, T. Taubner, F. Neubrech, and H. Giessen, Adv. Mater. **27**, 4597 (2015).
[37]E. T. Hu, T. Gu, S. Guo, K. Y. Zang, H. T. Tu, K. H. Yu, W. Wei, Y. X. Zheng, S. Y. Wang, R. J. Zhang *et al.*, Opt. Commun. **403**, 166 (2017).
[38]A. Pros and S. I. Bozhevolnyi, Opt. Express **21**, 27438 (2013).
[39]R. Smaali, F. Omeis, A. Moreau, T. Taliercio, and E. Centeno, Sci. Rep. **6**, 32589 (2016).
[40]G. Reed, G. Mashanovich, F. Y. Gardes, and D. J. Thomson, Nat. Photonics **4**, 518 (2010).
[41]S. Linden, C. Enkrich, M. Wegener, J. Zhou, T. Koschny, and C. M. Soukoulis, Science **306**, 1351 (2004).
[42]S. Zhang, W. Fan, K. J. Malloy, and S. R. J. Brueck, J. Opt. Soc. Am. B **23**, 434 (2006).
[43]K. Shportko, S. Kremers, M. Woda, D. Lencer, J. Robertson, and M. Wuttig, Nat. Mater. **7**, 653 (2008).
[44]X. Liu, T. Starr, A. F. Starr, and W. J. Padilla, Phys. Rev. Lett. **104**, 207403 (2010).
[45]B. J. Lee, L. P. Wang, and Z. M. Zhang, Opt. Express. **16**, 11328 (2008).
[46]Y. Bai, L. Zhao, D. Ju, Y. Jiang, and L. Liu, Opt. Express. **23**, 8670 (2015).
[47]J. Zhou, E. N. Economon, T. Koschny, and C. M. Soukoulis, Opt. Lett. **31**, 3620 (2006).
[48]J. Zhou, T. Koschny, M. Kafesaki, E. N. Economon, J. B. Pendry, and C. M. Soukoulis, Phys. Rev. Lett. **95**, 223902 (2005).